# Active Region Heating

Dr. Amy Winebarger

NASA MSFC

# Goals

- Overview of AR heating problem
- Highlight recent progress on AR heating from Hinode and IRIS
- What next?

# Why active region heating?

Active regions are a subset of coronal heating.

- Closed coronal structures
- Strong magnetic field

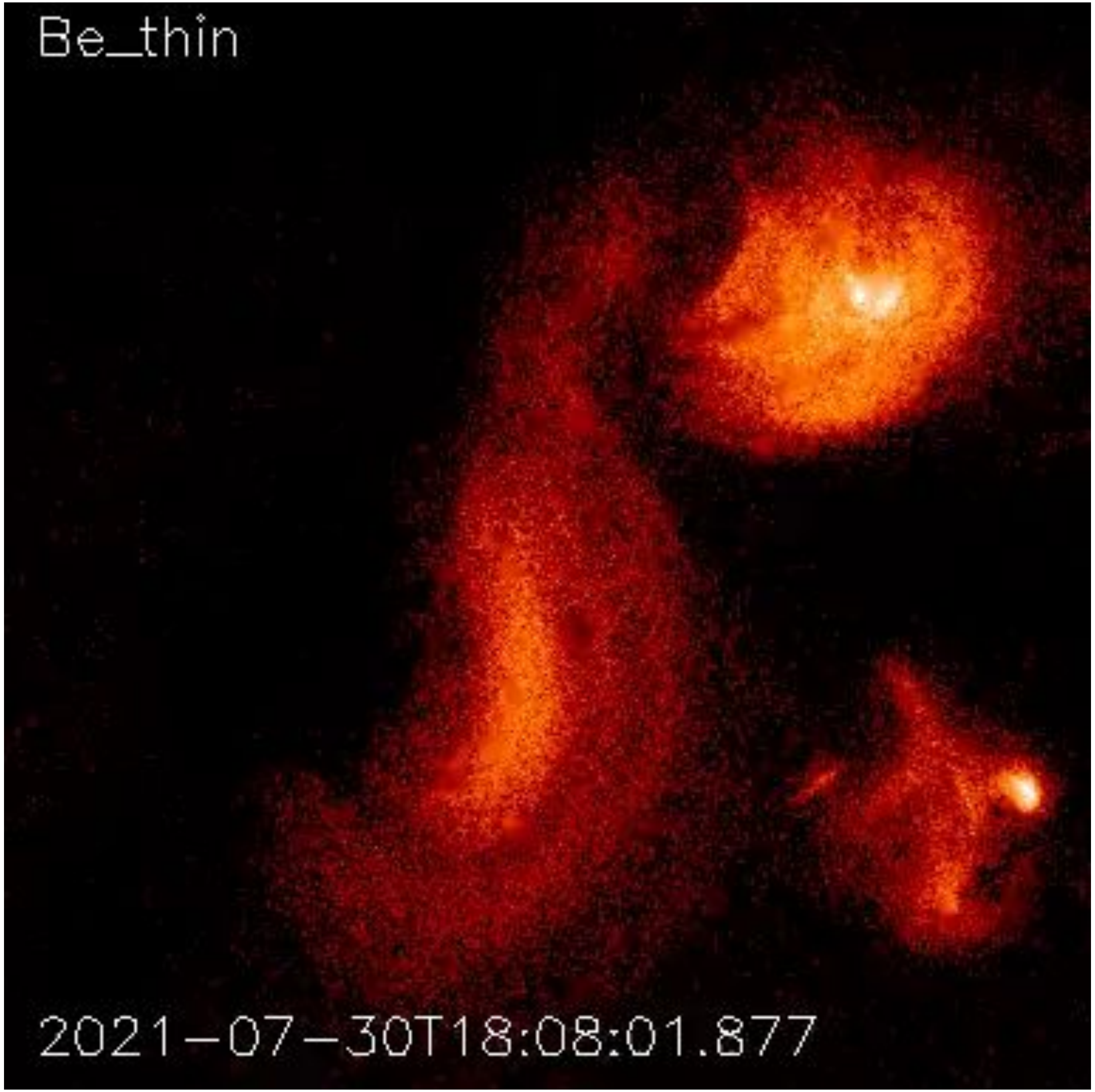

# Why active region heating?

Heating is:

- proportionate to magnetic field
- inversely proportionate to freedom of footpoint

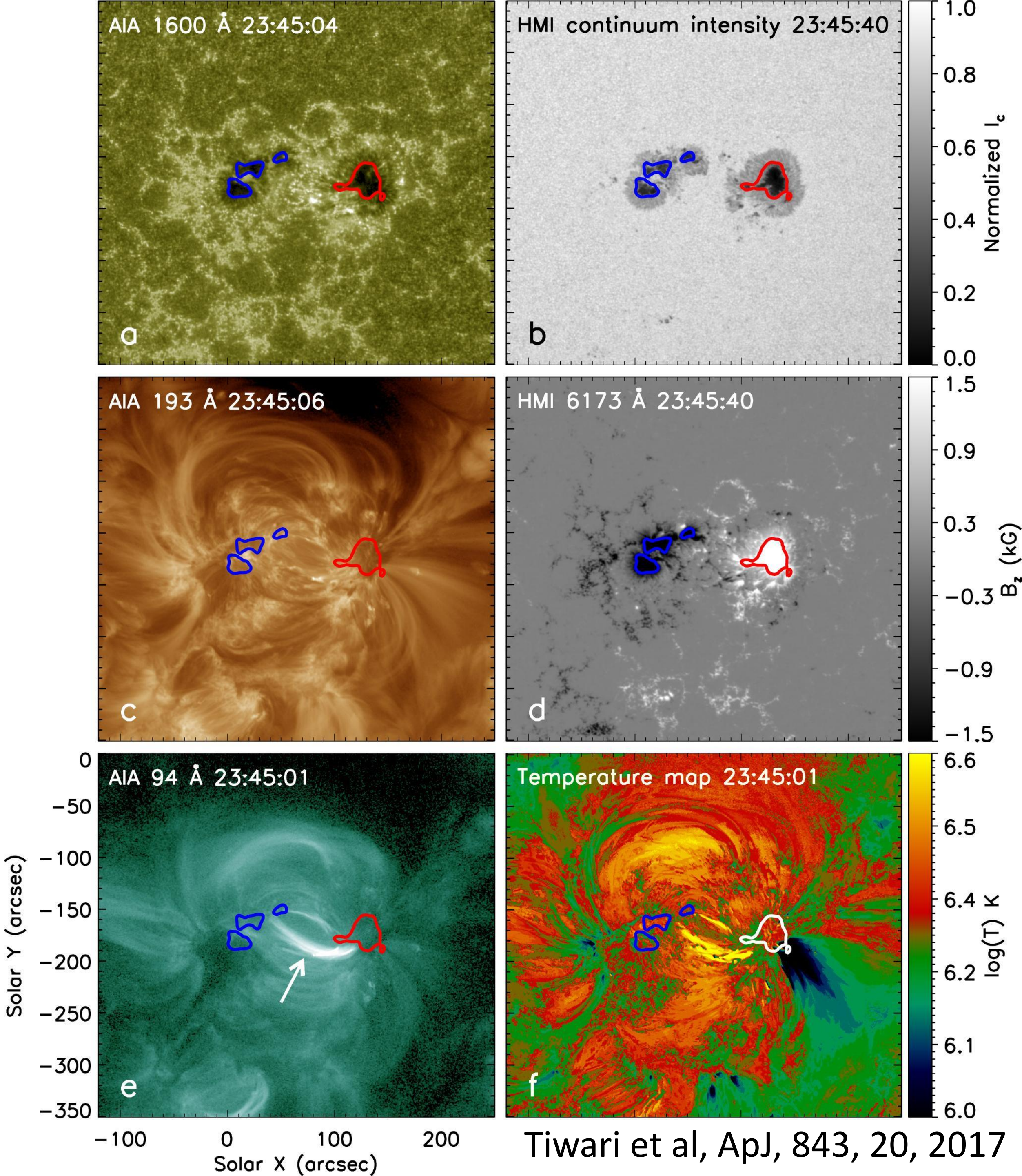


Tiwari et al, ApJ, 843, 20, 2017

# Active regions contain a broad temperature regime

Higher temperature observations are required

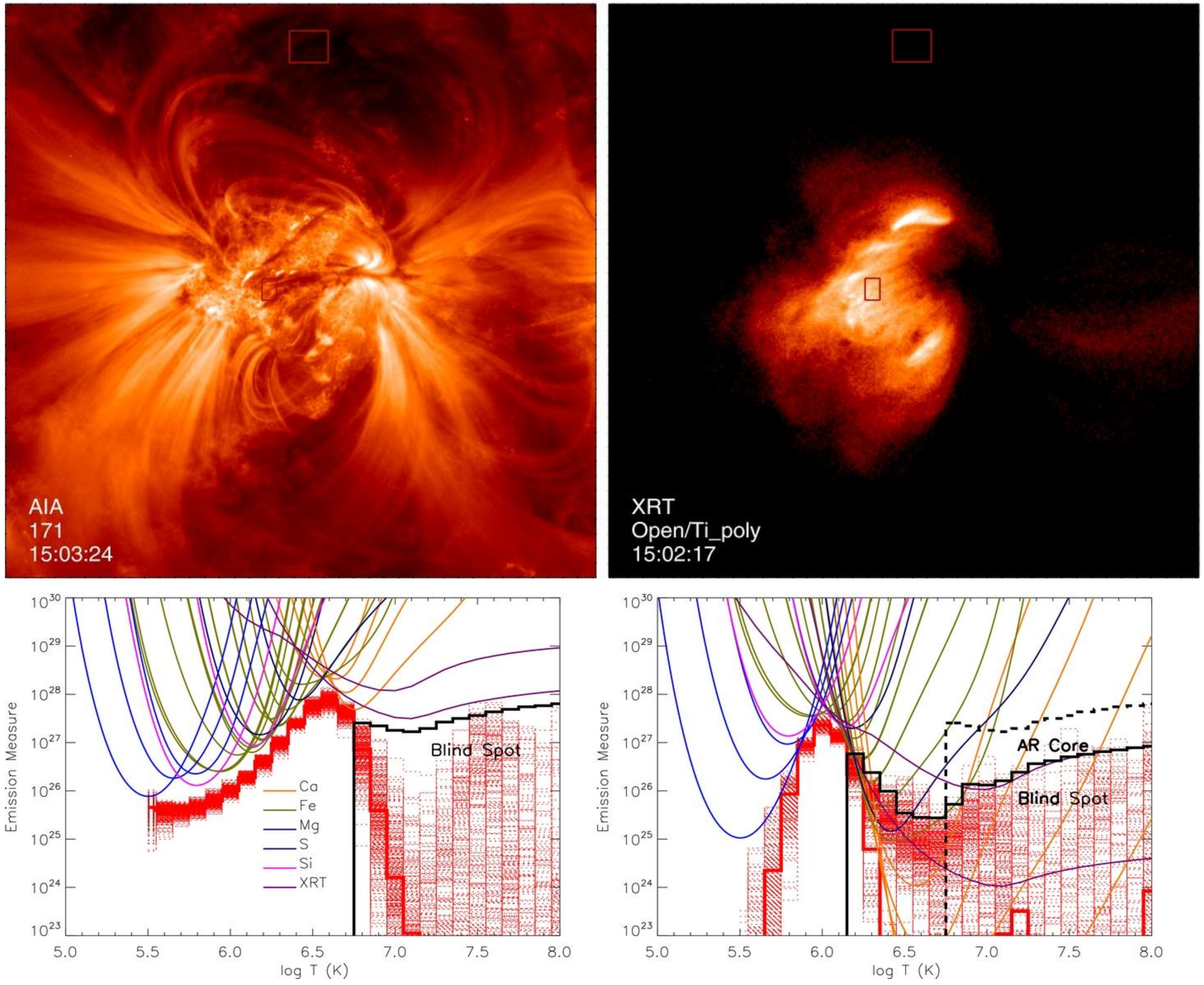


Winebarger et al, ApJL, 746, L17, 2012

# Active regions suffer from significant line-of-sight effects

Higher spatial resolution observations
Statistical studies
Spectral observations

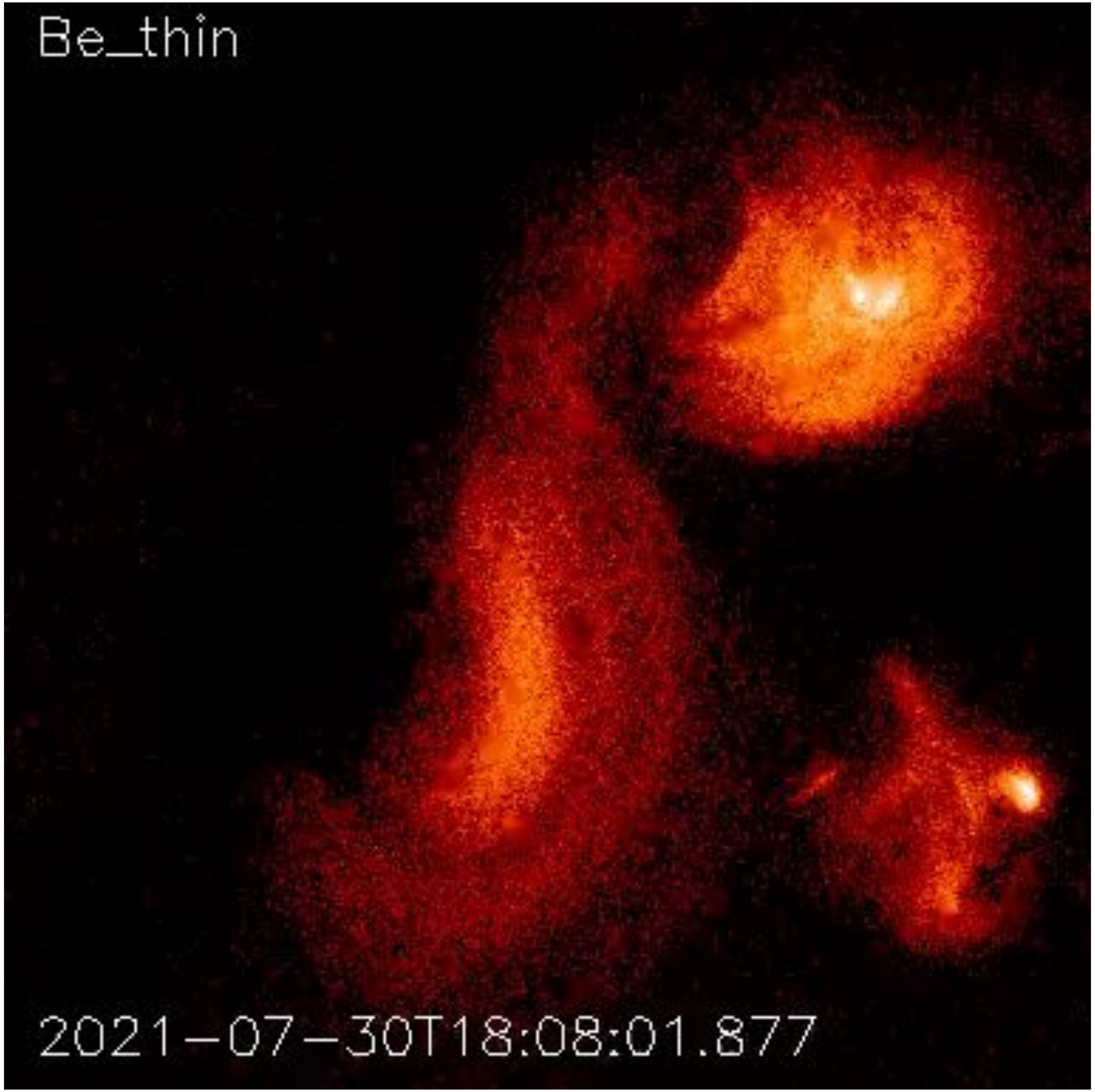

# Lots of Ideas

Difficult or impossible to measure quantities

Several models predict very similar observations

Discriminating Observations

**Table 1 MHD coronal heating theories: Efficiency scalings relative to the Poynting flux**

| Model description | Efficiency ($\mathcal{E}$) | Example reference |
|---|---|---|
| | Wave Dissipation (AC) Models | |
| Alfvén-wave collisional damping | $\Lambda^1 \Theta^2 Re^{-1}$ | Osterbrock (1961) |
| Resonant absorption | $\Lambda^1 \Theta^1$ | Ruderman et al. (1997) |
| Phase mixing | $\Lambda^1 \Theta^{4/3} Re^{-1/3}$ | Roberts (2000) |
| Surface-wave damping | $\Lambda^{1/2} \Theta^{3/2} (\Sigma / Re)^{1/2}$ | Hollweg (1985) |
| Fast-mode shock train | $\Lambda^2 \Theta^3$ | Hollweg (1985) |
| Switch-on MHD shock train | $\Lambda^3 \Theta^4$ | Hollweg (1985) |
| | Turbulence Models | |
| Kolmogorov-Obukhov cascade | $\Lambda^1 \Theta^2$ | Hollweg (1986) |
| Iroshnikov-Kraichnan cascade | $\Lambda^2 \Theta^3$ | Chae et al. (2002) |
| Hybrid triple-correlation cascade | $\Lambda^1 \Theta^3 (1+\Theta)^{-1}$ | Zhou & Matthaeus (1990) |
| Reflection-driven cascade | $\Lambda^1 \Theta^2 (f_+^2 f_- + f_-^2 f_+)$ | Hossain et al. (1995) |
| 2D boundary-driven cascade | $\Lambda^{2/3} \Theta^{1/3}$ | Heyvaerts & Priest (1992) |
| Line-tied reduced MHD cascade | $\Lambda^1 \Theta^{1/2}$ | Dmitruk & Gómez (1999) |
| | Footpoint Stressing (DC) Models | |
| Current-layer random walk | $\Lambda^1$ | Sturrock & Uchida (1981) |
| Current-layer shearing | $\Lambda^1 (1+\Theta^2)^{1/2} (1+\Lambda^2)^{-1/2}$ | Galsgaard & Nordlund (1996) |
| Braided discontinuities | $\Lambda^2 \Theta^1$ | Parker (1983) |
| Flux cancellation | $\Lambda^1 \Theta^1 (\phi^{8/3} - \phi^{4/3})$ | Priest et al. (2018) |
| | Taylor Relaxation Models | |
| Tearing-mode reconnection | $\Lambda^1 \Theta^1 (1-\alpha L)^{-5/2}$ | Browning & Priest (1986) |
| Hyperdiffusive reconnection | $\Lambda^1 \Theta^{-1} (\alpha L)^2$ | van Ballegooijen & Cranmer (2008) |
| Non-ideal/slipping reconnection | $\Theta^{-1} (\alpha L)^1$ | Yang et al. (2018) |

Cranmer & Winebarger, Annual Review of Astronomy and Astrophysics, vol. 57, p.157-187, 2019

# Determining Discriminating Observations

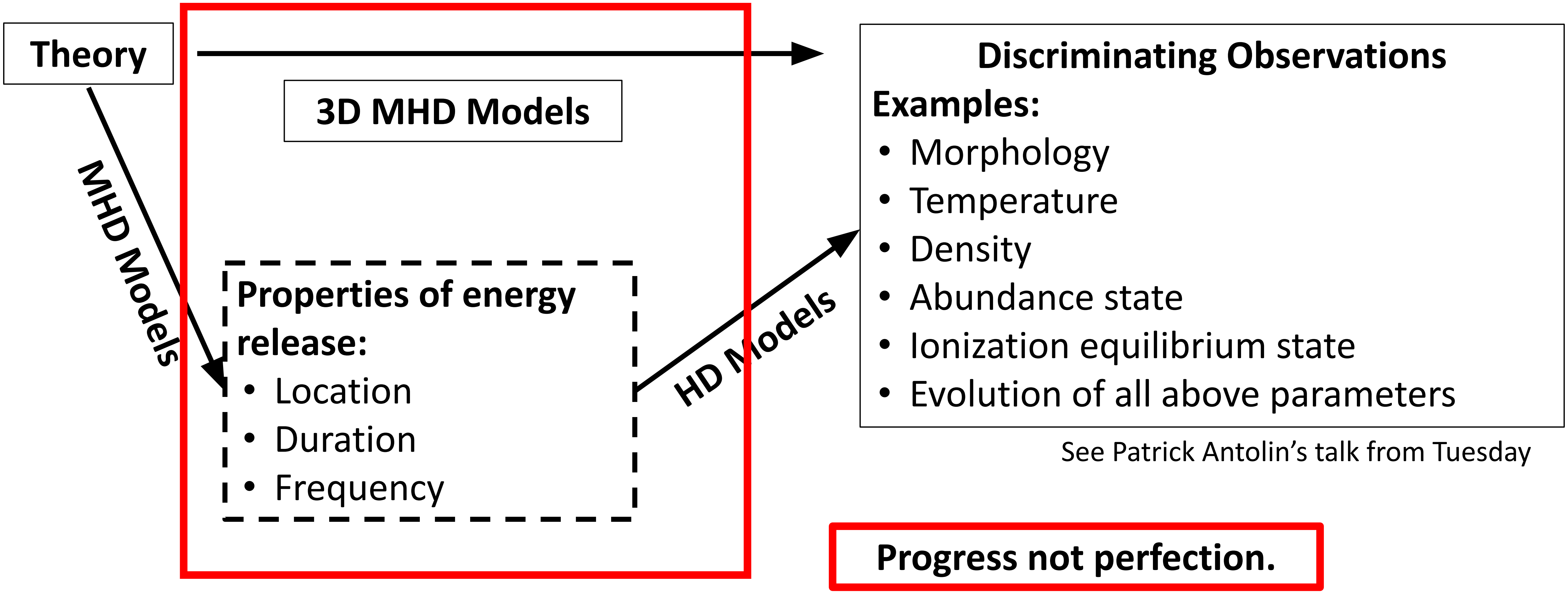

# Direct Discriminating Observations

Very few direct observations of braiding.

Hi-C 1 observation is the exception.

Limited evidence that braiding at this scale is prevalent.

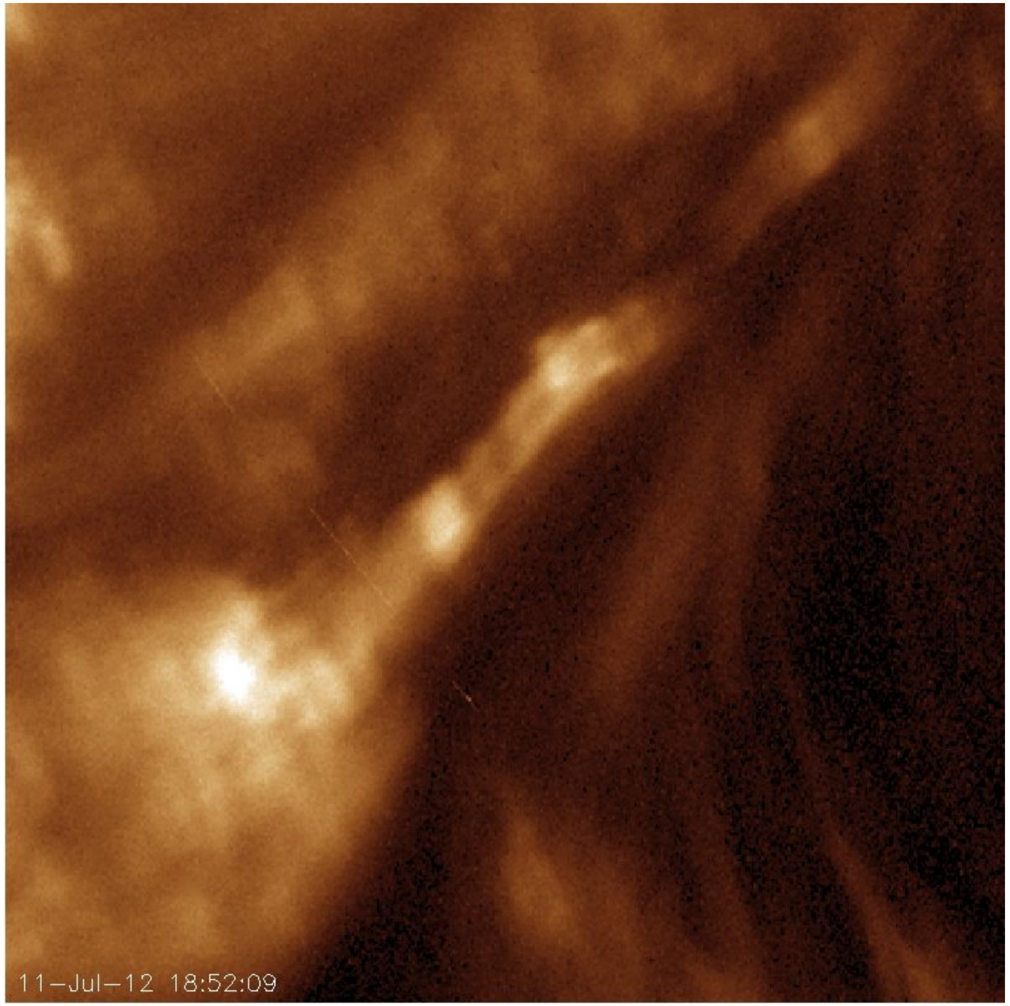

# Chromospheric Response to Reconnection from IRIS

- Chromospheric response can be used to determine heating parameters.
- Consistent with short term heating in corona.

Testa et al, 2014, Science, 346, 6207
Testa et al. 2020, ApJ, 889, 124

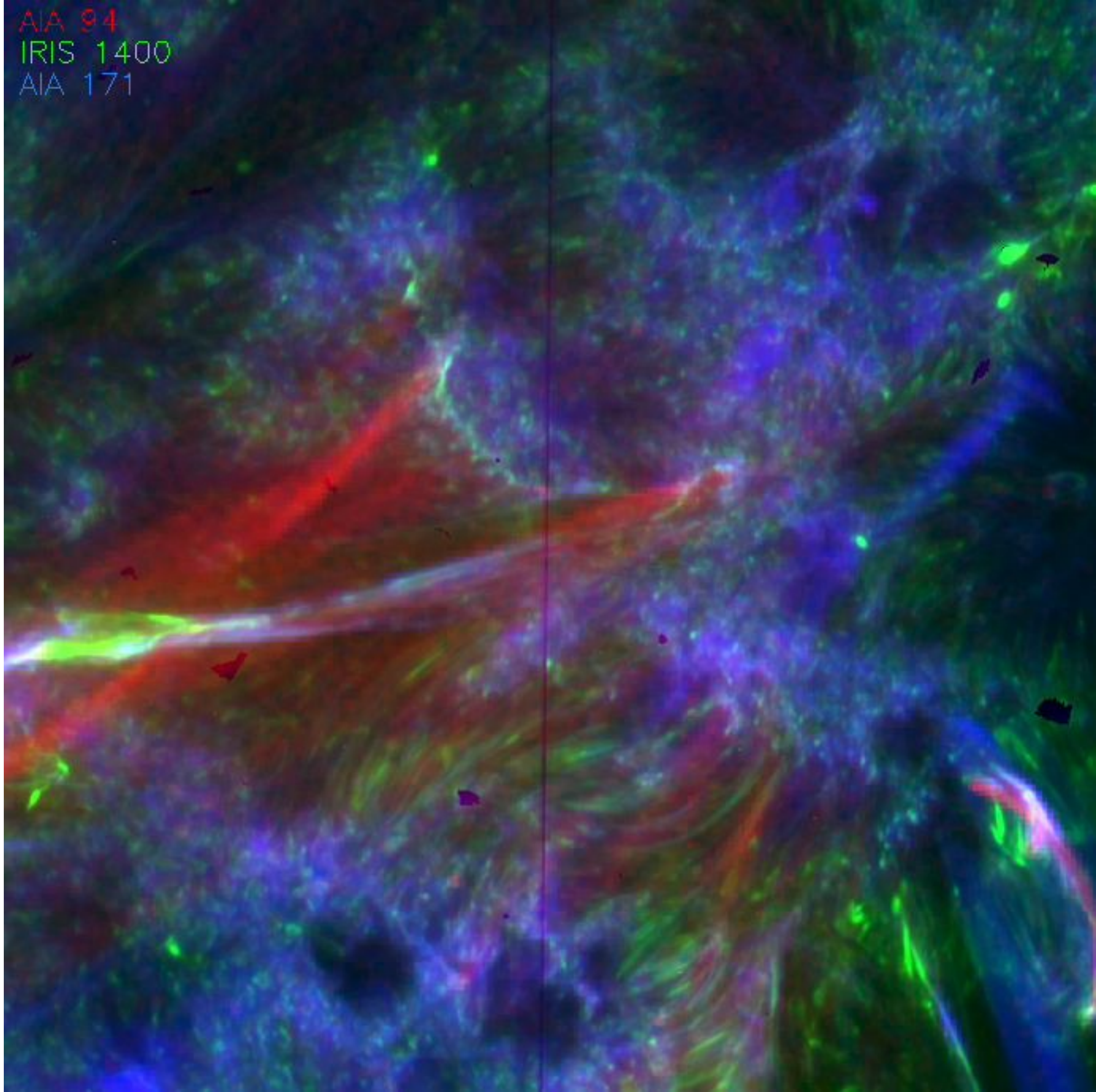

# Nanojets in IRIS

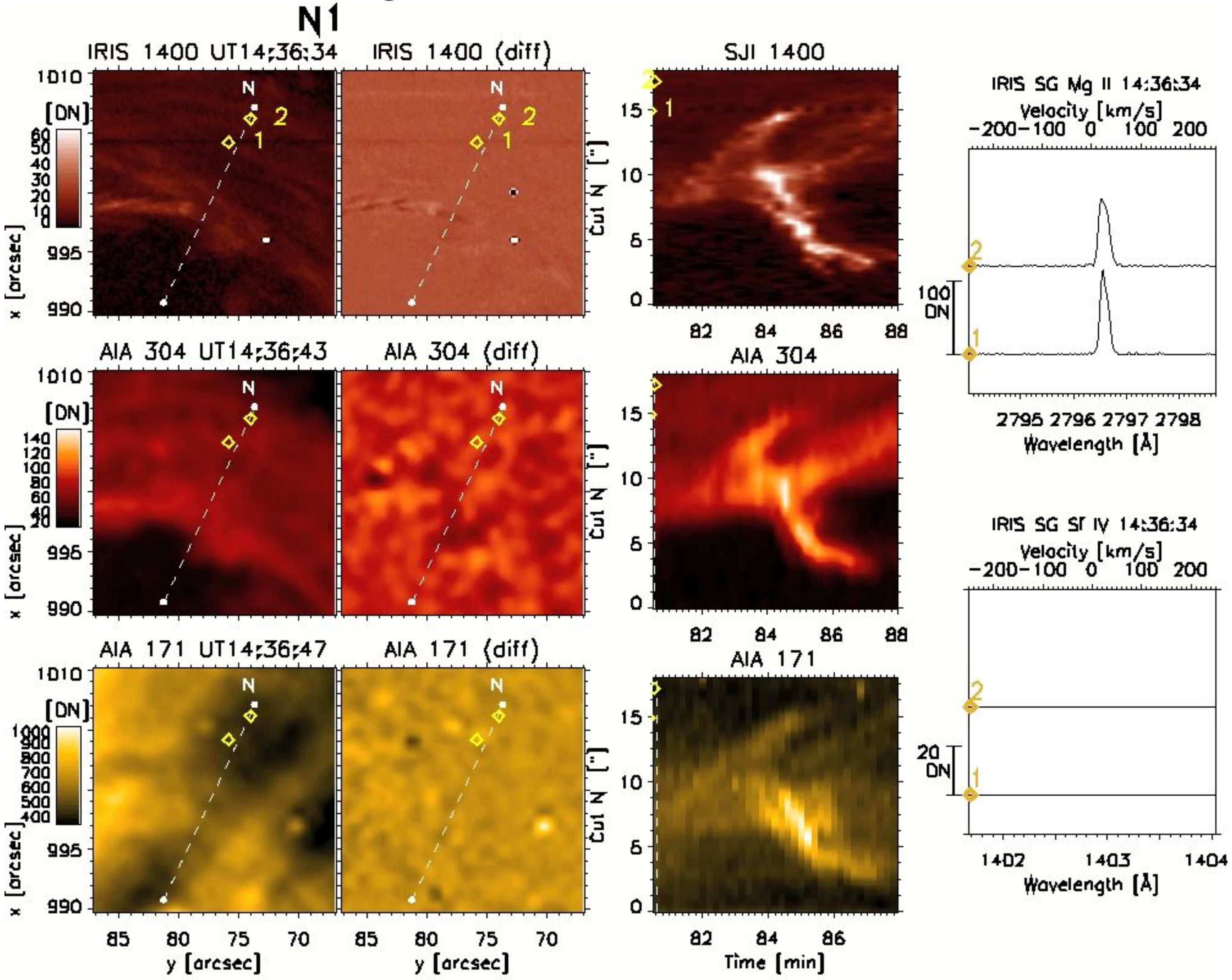


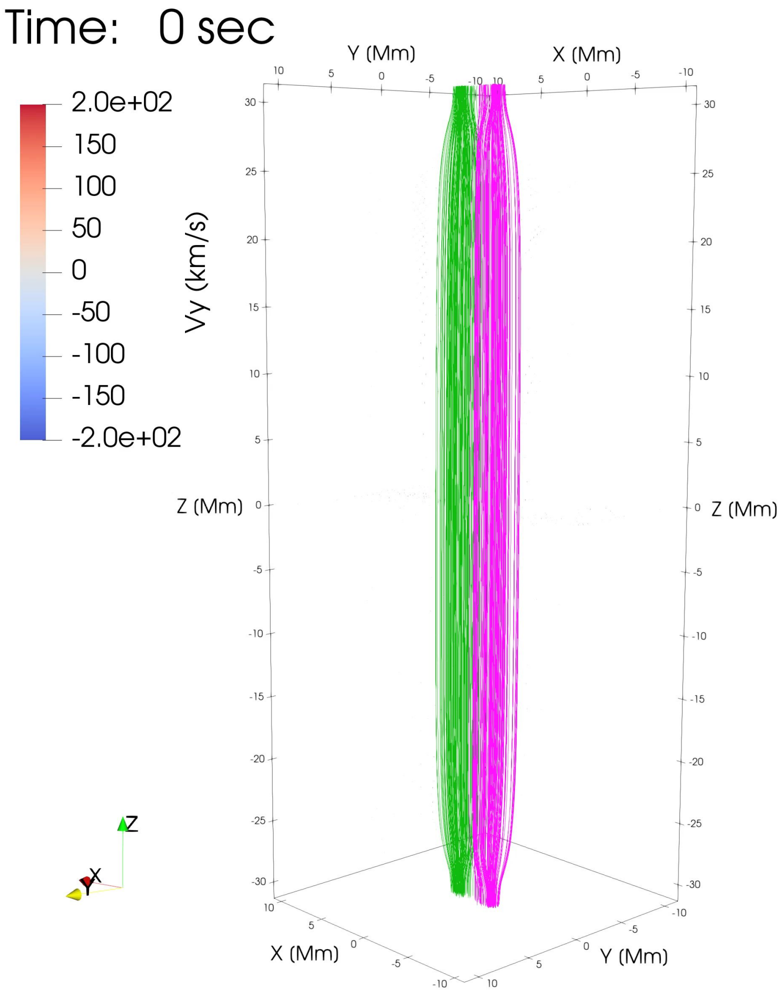


Observations support magnetic reconnection in corona.

Antolin et al, 2021, Nature Astronomy, 5, 54

# Heating frequency heating related to EM slope

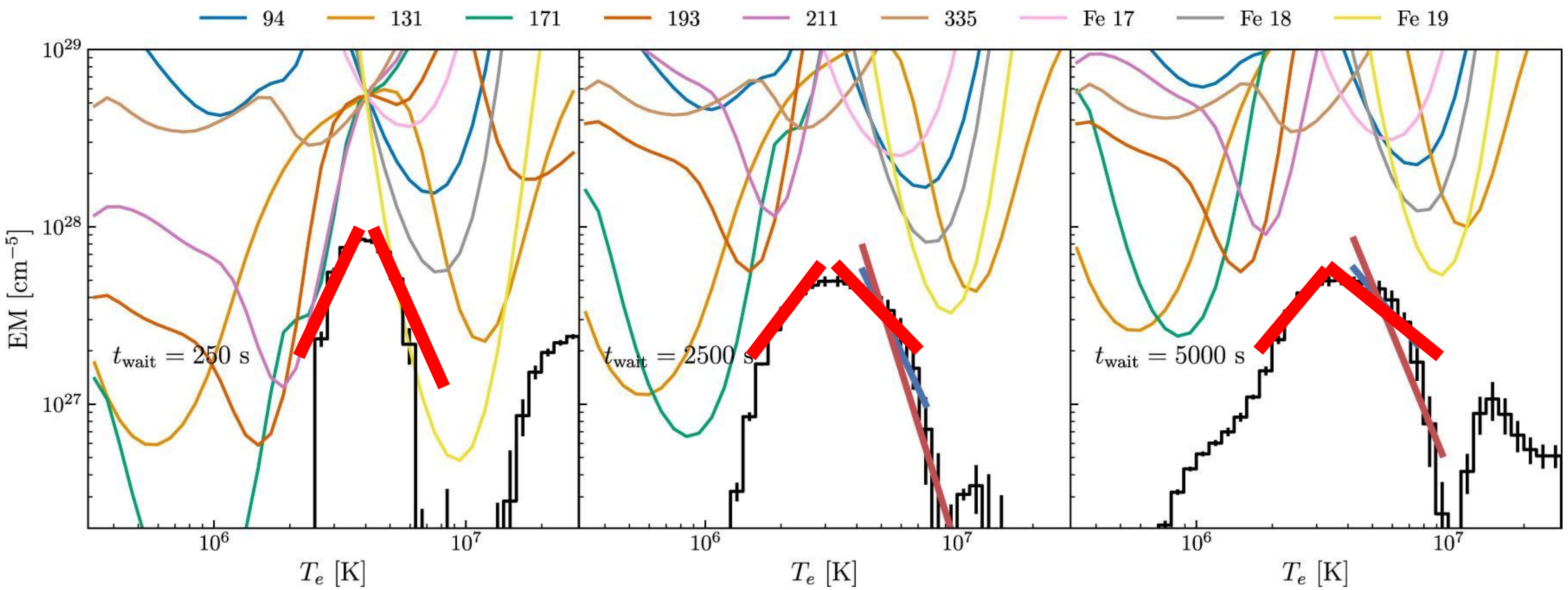


**High Frequency**
Larger alpha and beta

**Low Frequency**
Smaller alpha and beta

Athiray et al., ApJ, 2019, 884, 24

# Cool EM slope from EIS

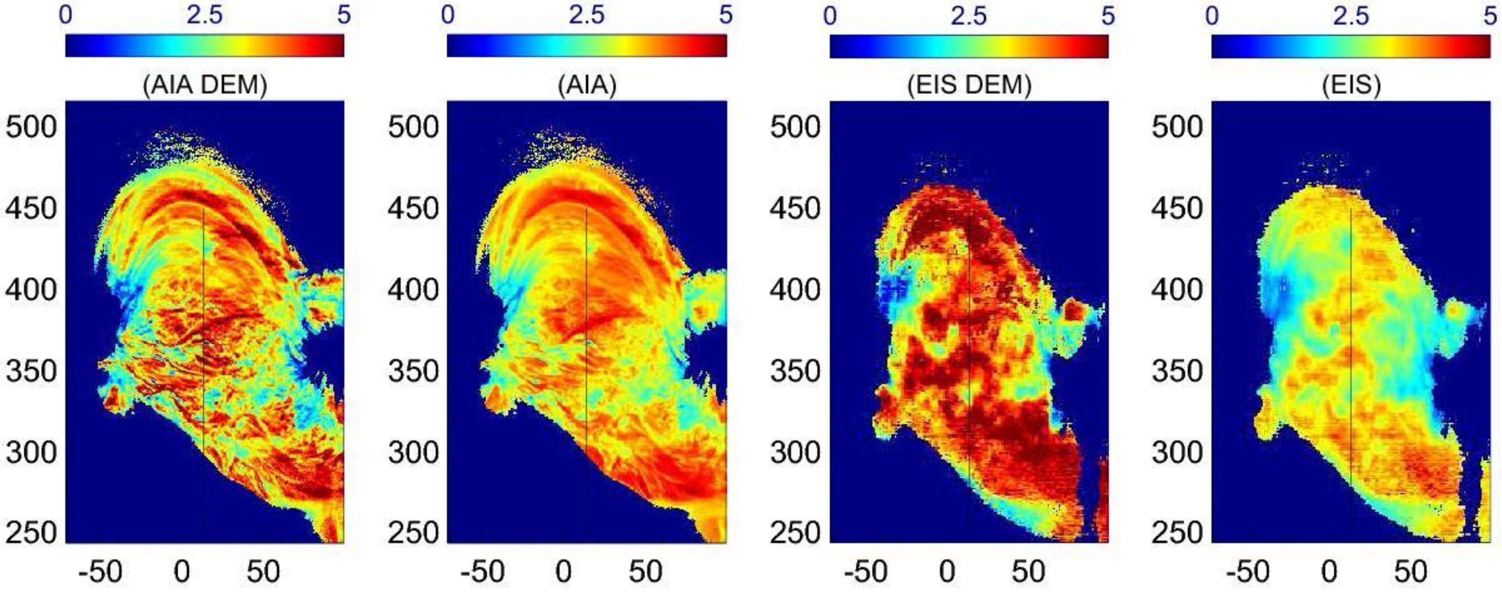


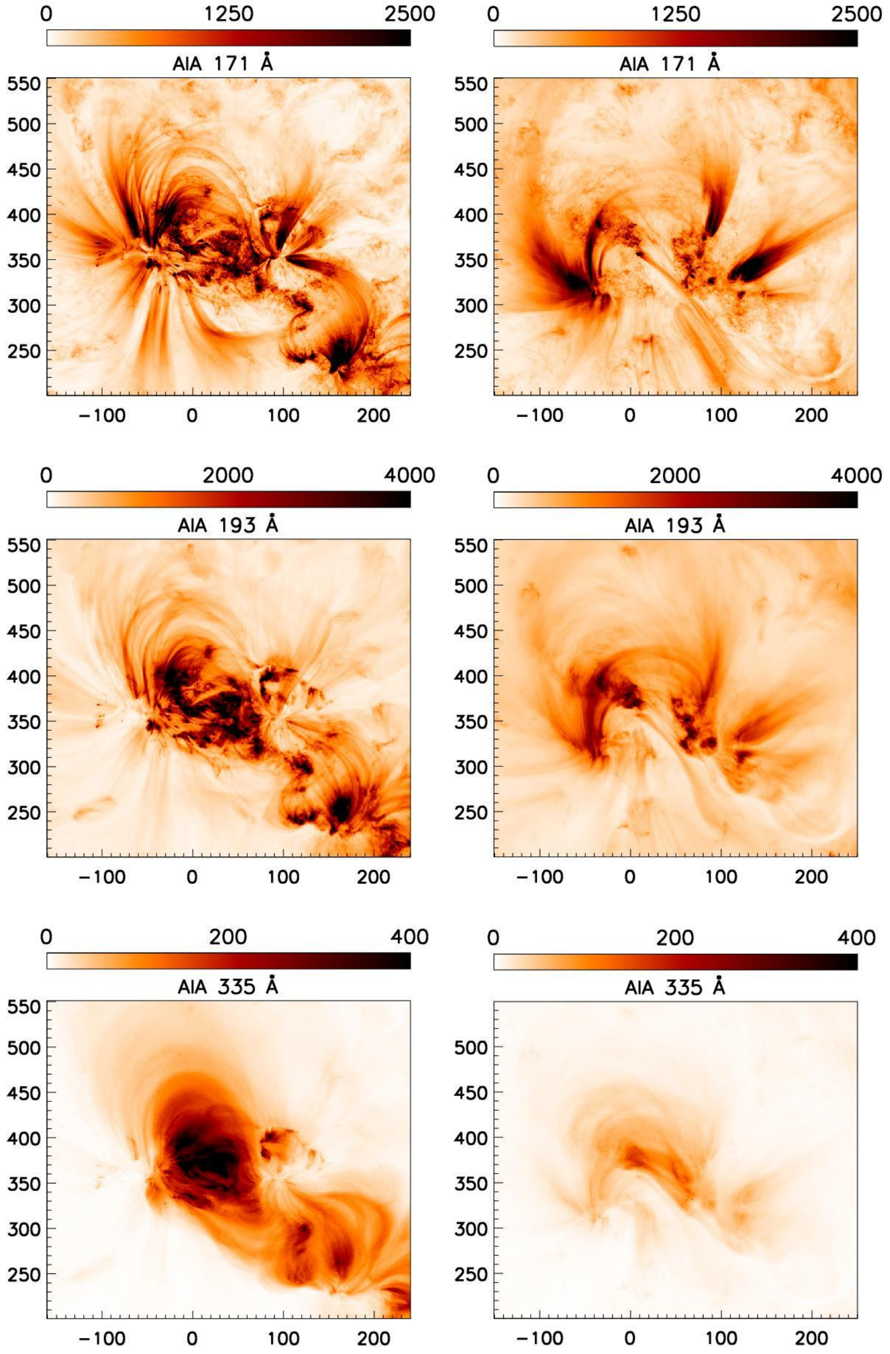


- Single active region, two rotations
- Emission Measure fit from 1-3 MK
- Consistent with high frequency heating

Del Zanna et al., A&A 573, A104 (2015)

# High Temperature EM slope from EIS

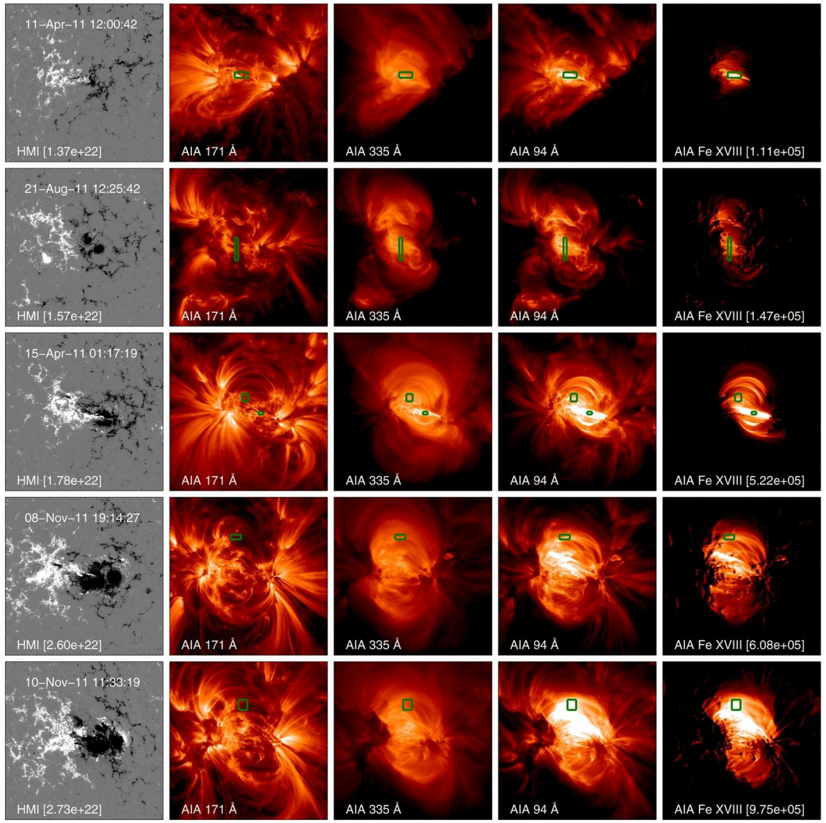


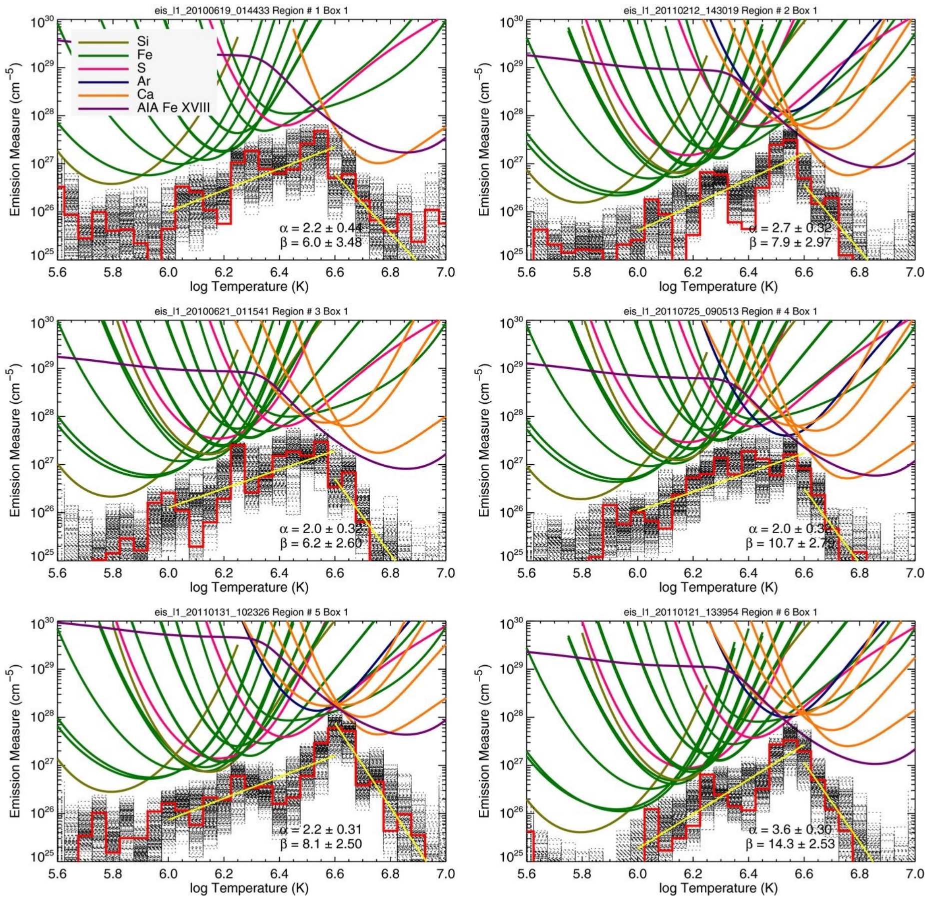


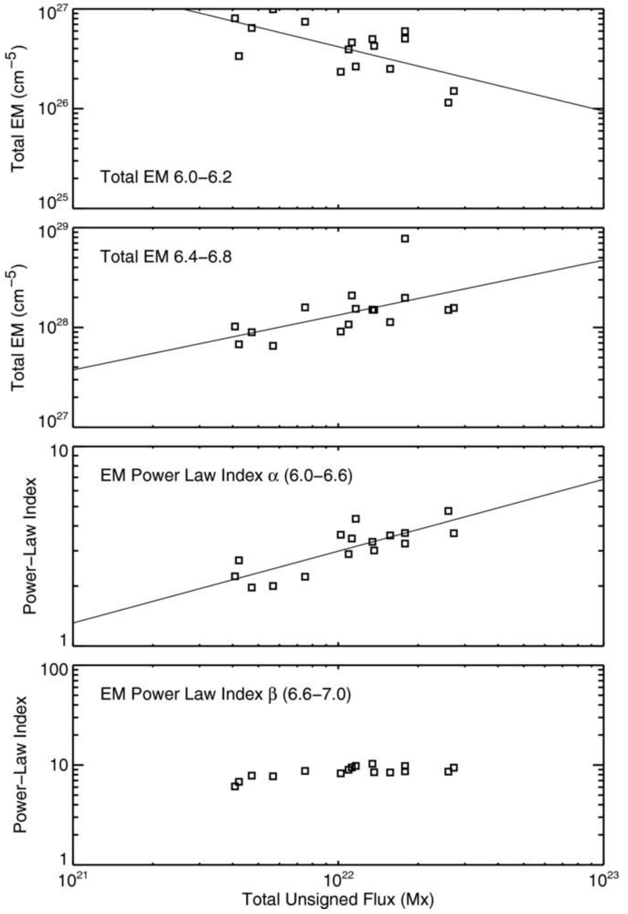


- 15 active regions
- Emission Measure fit from 6.0 – 6.6 and 6.6-7.0
- Consistent with high frequency heating

Warren, Winebarger, & Brooks 2012 *ApJ*, **759** 141.

# Nonthermal Velocity from EIS

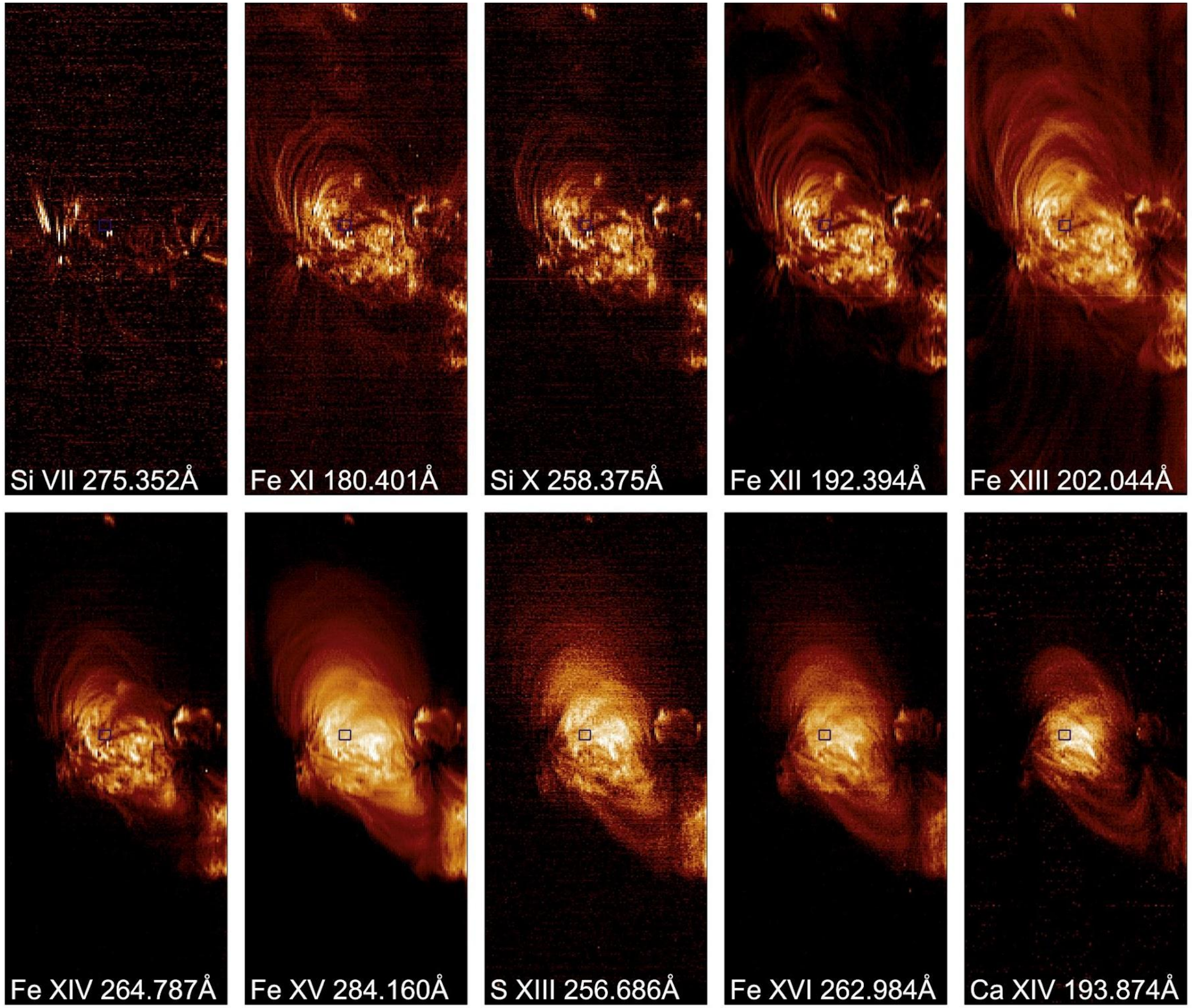


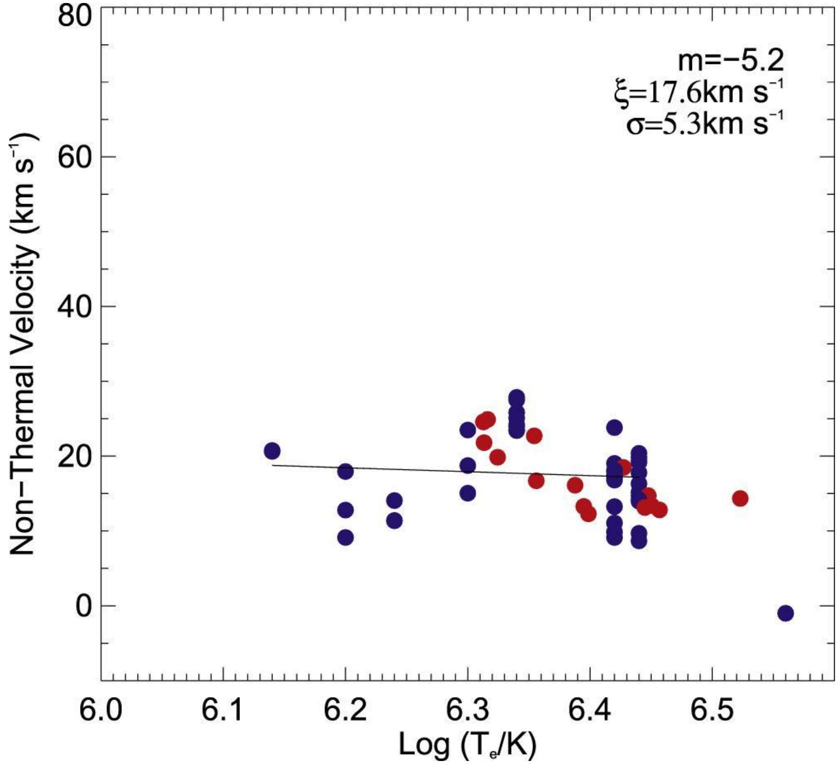


- Survey of 15 active regions
- Modest NT velocities
- No temperature or magnetic field dependence
- Inconsistent with most coronal heating models

Brooks & Warren, 2016, ApJ, 820, 63

# What's next?

- Higher spatial resolution (IRIS/Hi-C like)
- Broader temperature coverage
- More (larger FOV) spectral coverage

# Future missions:

- EUVST (funded)
- MUSE (proposal)
- EUNIS, MaGIXS, FOXSI -type mission (pre-formulation)

# MUSE

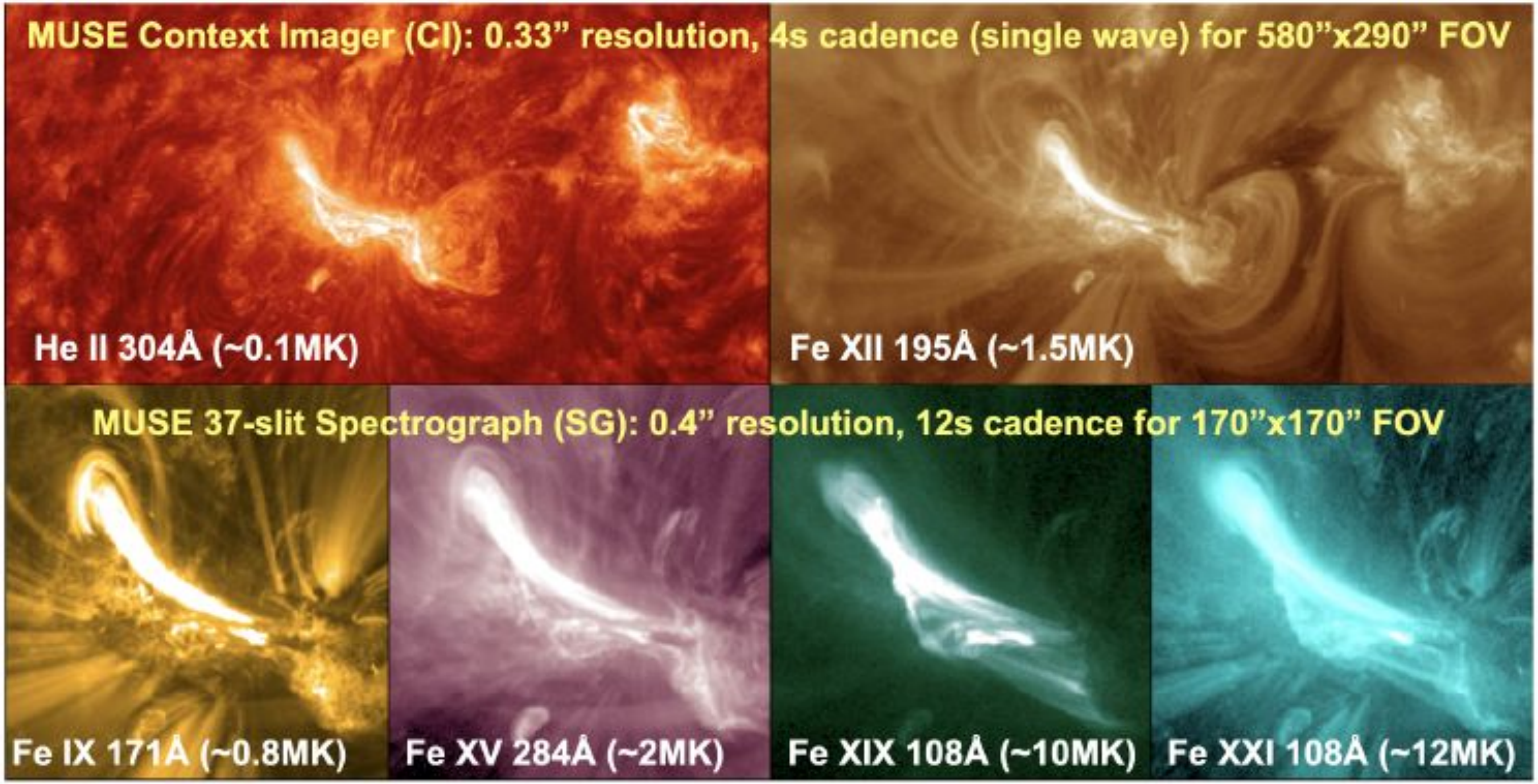


De Pontieu et al, ApJ, accepted, 2021

# MUSE

**Table 3.** Predicted *MUSE* diagnostics for various models of heating mechanisms

| Mechanism | Predicted Diagnostic | $\lambda^*$ [Å] | Figures |
|---|---|---|---|
| Spicules | - type I and type II spicules | 304 | 2, 3 |
| | - short-lived blue-shifted brightenings at loop footpoints associated w/ spicules | 171 | 2, 3 |
| | - propagation of Alfvénic waves (Doppler and POS motions), triggered by spicules, along loops | 304, 171, 195, 284 | 13a, 16-18 |
| | - dissipation of Alfvénic waves through impulsively-driven KHI | 171, 284 | 13, 16-18 |
| | - formation of coronal loop, associated with spicules | 171, 195, 284 | 2, 3 |
| | - evaporative flows at loop footpoints, associated with spicules | 284 | 2, 3 |
| Braiding | - visibly braided loops | All | 7 |
| | - spatio-temporal coherence of intensity and line width along loops (20-60s, $\sim$ 5-30″) | 171, 284, 108 | 4, 5, 10 |
| | - short-lived ($\approx$ 20s single, $\approx$ 60s cluster) nanojets: high velocities ($<\sim$ 100 km $s^{-1}$) and line widths, transverse to guide field | 171, 284, 108 | 4, 8, 9 |
| | - loop formation associated with nanojets | 171, 195, 284, 108 | 8 |
| | - twisting and unwinding motions | 171, 195, 284 | 7 |
| | - evaporative flows in loops | 171, 284, 108 | 6, 10, 11 |
| | - nanoflare driven short-lived brightenings at loop footpoints, and associated short-lived hot loop emission | 171, 284, 108 | 10, 11 |
| Waves | - propagating or standing oscillatory displacements of loops and jets | 304, 171, 195, 284 | 16-19 |
| | - oscillations in velocity, line width along loops | 171, 284 | 12-14,16-19 |
| | - spatial dependence of FFT power spectrum along loop | 171, 284 | 13 |
| | - propagation of Doppler shift oscillations along loops | 171, 284 | 14, 16-18 |
| | - spatio-temporal coherence of velocities and line width along loops from wave propagation | 171, 284 | 12, 14, 16-18 |
| | - specific phase relationships between intensity, velocity, line width | 171, 284 | 16-19 |
| | - concentration of wave power at edge of flux tubes (KHI, RA) | 171, 195, 284 | 16-18 |
| | - steady downflows/upflows around edge of flux tubes (KHI, RA) | 171, 195, 284 | 16-18 |
| Flux Emerg. | - short-lived, low-lying loops, possible EUV absorption from overlying cool plasma | 304, 171, 195, 284 | 20 |
| | - flow patterns associated with draining of rising loops and topological evolution including footpoint separation | 171, 284, 195 | 20, 21 |
| | - strong short-lived brightenings and bi-directional flows ($>$ 100 km $s^{-1}$), large line widths (from large-angle reconnection) | 171, 284, 108 | 20, 21 |
| | - spatio-temporal coherence of highly dynamic "storms" of sudden brightenings and line width increase (10-30″, 20s) | 304, 171, 195, 284, 108 | 20, 21 |
| | - various types of jets, including erupting (mini-)filaments | 304, 171, 195, 284 | 20, 21 |

*For 304 and 195 imaging is desired. For 171, 284, and 108, intensity, Doppler shift, and line broadening are typically desired.

De Pontieu et al, ApJ, accepted, 2021

# MaGIXS

Relative high temperature emission **discriminates** the heating frequency

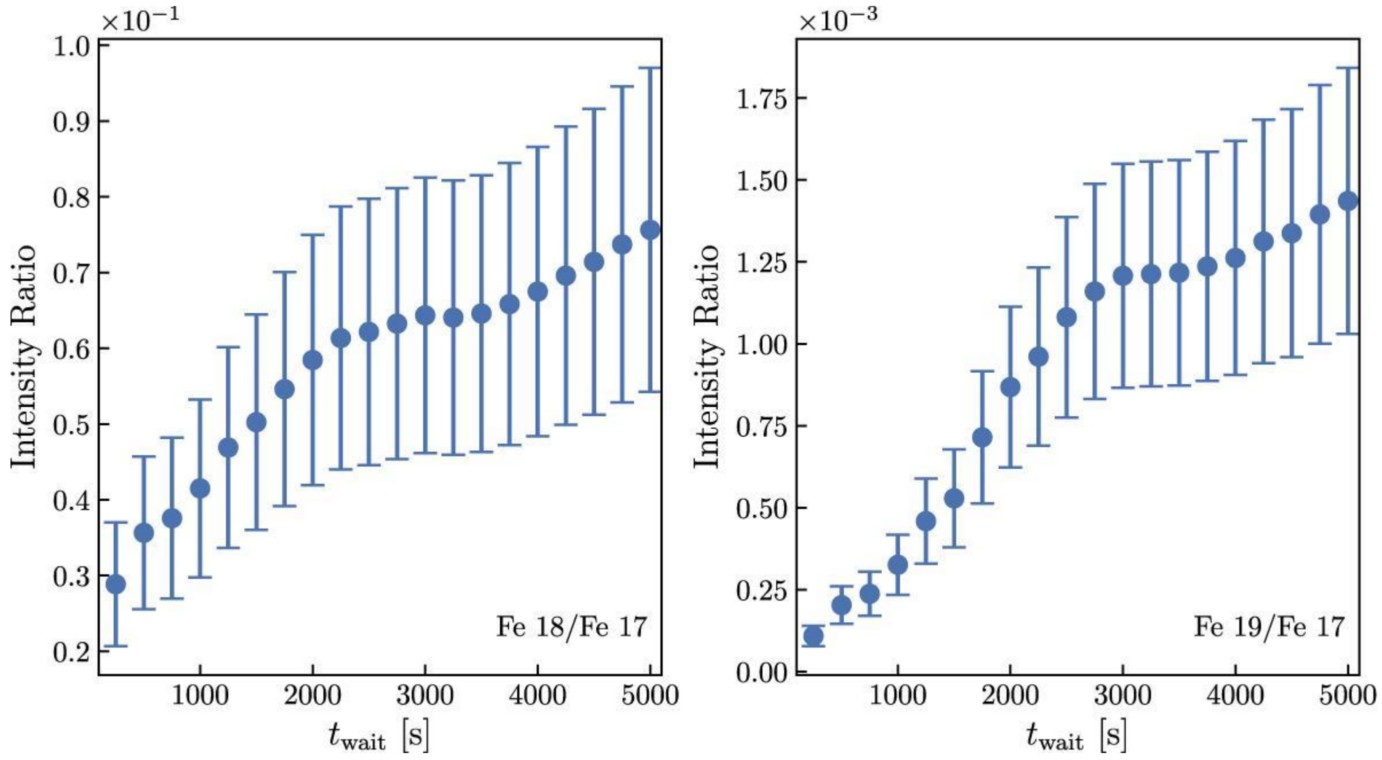


| Ion | Wavelength (A) | Log Max Temperature |
|---|---|---|
| FeXVII | 15.01 | 6.6 |
| FeXVIII | 14.21 | 6.8 |
| FeXIX | 13.53 | 6.95 |
| Ne IX | 13.45 | 6.6 |
| O VII | 21.60 | 6.3 |

Athiray et al., ApJ, 2019, 884, 24

# FOXSI

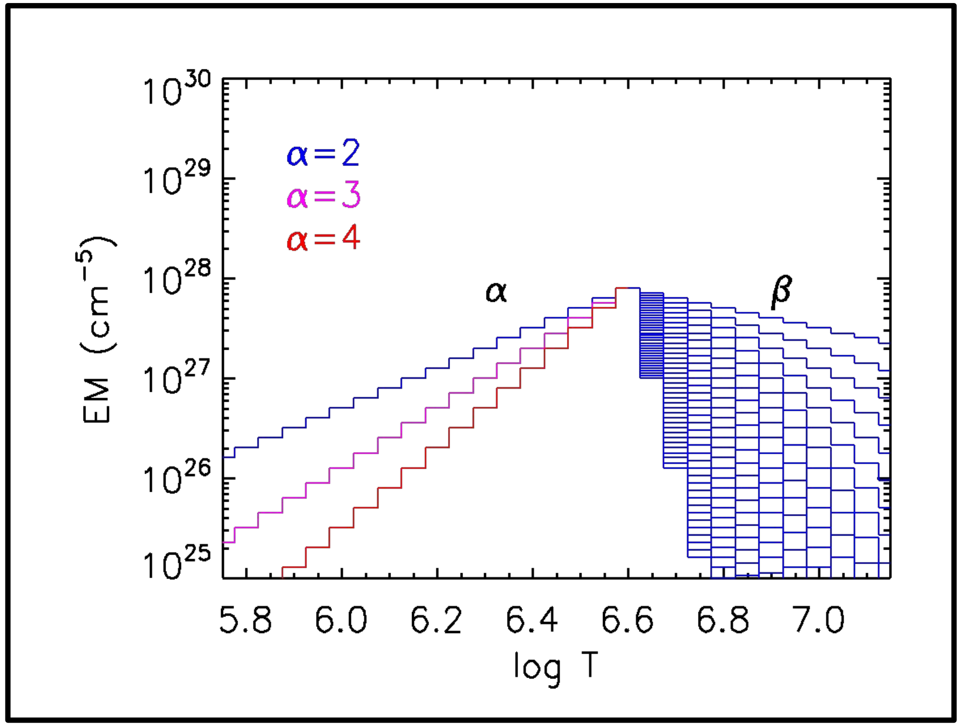


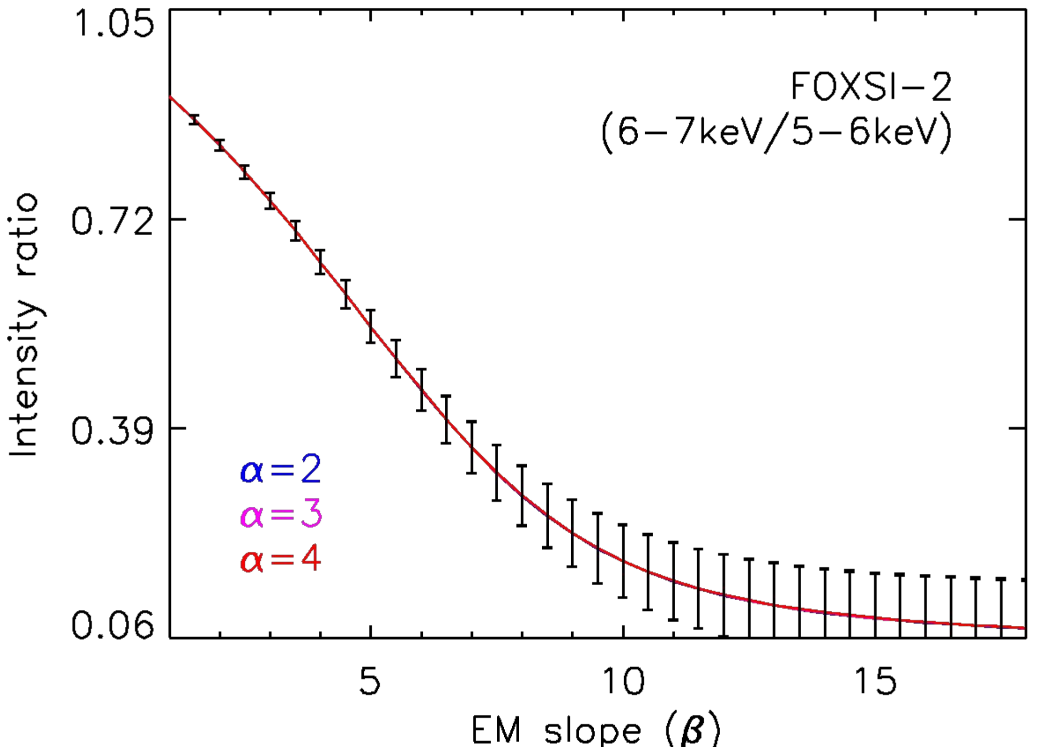


FOXSI-2 intensity ratio is insensitive to α, strongly vary with β .

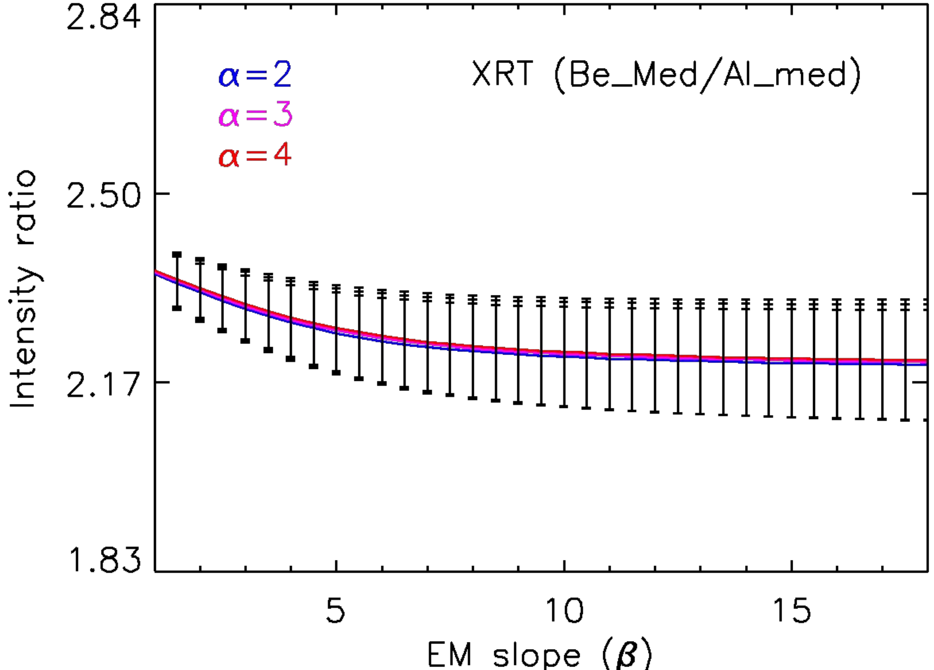


The intensity ratios of the two XRT channels are insensitive to β.

Athiray et al., ApJ, 2019, 884, 24